


Quantum simulation of bound-state-enhanced quantum metrology

Cheng-Ge Liu,^{1,*} Cong-Wei Lu,^{1,*} Na-Na Zhang²,[✉] and Qing Ai^{1,†}

¹*Department of Physics, Applied Optics Beijing Area Major Laboratory, Beijing Normal University, Beijing 100875, China*

²*School of Optoelectronics Engineering, Chongqing University of Posts and Telecommunications, Chongqing 400065, China*

 (Received 23 November 2023; revised 8 March 2024; accepted 5 April 2024; published 26 April 2024)

Quantum metrology explores quantum effects to improve the measurement accuracy of some physical quantities beyond the classical limit. However, due to the interaction between the system and the environment, the decoherence can significantly reduce the accuracy of the measurement. Many methods have been proposed to restore the accuracy of the measurement in the long-time limit. Recently, it was found that the bound state can help improve measurement accuracy and recover the t^{-1} scaling [Bai *et al.*, *Phys. Rev. Lett.* **123**, 040402 (2019)]. Here, by using N qubits, we propose a method to simulate the open quantum dynamics of a hybrid system including one atom and coupled resonators. We find that the error of the measurement can decrease as the time increases due to the existence of the bound state. With both analytical and numerical simulations, we prove the t^{-1} scaling of the measurement error can be recovered when there is a bound state in the hybrid system. Interestingly, we observe that there are regular oscillations which can be used for the evaluation of the atomic transition frequency. For a finite N , the duration of the regular oscillations doubles as one more qubit is involved.

DOI: [10.1103/PhysRevA.109.042623](https://doi.org/10.1103/PhysRevA.109.042623)

I. INTRODUCTION

Compared with classical metrology, quantum metrology can greatly improve measurement accuracy and can play a significant role in gravitational-wave detection [1–3] and quantum radar [4–6], atomic clocks [7–10], magnetometers [11–13], gravimeters [14,15], navigation and biological monitoring [16–21], quantum biology [17–19], and so on. According to the central-limit theorem [22,23], if one performs a large number of measurements, the error of the measurements will be reduced by a factor \sqrt{M} , with M being the number of measurements, i.e., the shot-noise limit (SNL) or the standard quantum limit [23]. Quantum metrology explores quantum entanglement [24–26], coherence [27–29], and squeezing [30–32] to improve the accuracy of the measurement in order to reach the Heisenberg limit (HL), which scales as M^{-1} . As long as the system-bath interaction is present, the measurement of a specific physical quantity is inevitably affected by the error. The precision of quantum metrology in a Markovian bath is reduced to the SNL [33]. The SNL can also be overcome in non-Markovian noise and can thus achieve the Zeno limit (ZL), i.e., $M^{-3/4}$ [34–36].

The Ramsey spectrum is widely used in practical quantum metrology, which approaches the HL when noise is absent [37]. However, in practice, since the system is open to the environment, the measurement accuracy of physical quantities will be affected by environmental noise. In the presence of Markovian pure-dephasing noise, the accuracy is reduced from the HL back to the SNL [33]. Although under non-Markovian noises the accuracy can reach the ZL, it is still

lower than the HL [35,36,38,39]. In both cases, the measurement error will diverge over time. In order to improve the measurement accuracy, many methods have been proposed, such as purification [40], error correction [41–43], nondegenerate measurements [44], and bound states outside the continuum [23,45]. None of these proposals recover the HL, and they especially fail to resolve the issue of error diverging over time. It is natural to ask the question of how one can restore the measurement error without it diverging over time.

Recent studies have shown that when there is a bound state in the open quantum system, it allows the measurement precision to beat the SNL and recover the ZL over long encoding times [45]. The bound state is an interesting state that can be observed in the boson-impurity model in which two-level systems are coupled to a boson bath. Here, the impurity is the emitter (e.g., atom), and the boson bath is the electromagnetic-field mode [46]. Bound states can possess many interesting phenomena, such as fractional decay, localized phase transitions [46], Cooper pairs in superconductivity [47], and polarons in electron transport [48]. On the other hand, we notice that a hybrid system including a few atoms and a coupled cavity array has been extensively studied in the past decade. It can be used for single-photon switch [49,50], quantum transistors [51], routers [52], supercavities [53], nonreciprocal optics [54], and frequency converters [55]. Inspired by these discoveries, in this paper, we propose a scheme to simulate the open quantum dynamics of an atom in coupled resonators. Here, the coupled resonators form a structured bath with the energy band centered at the cavity frequency and a bandwidth 4 times the intercavity coupling. When the atomic transition frequency lies within the energy band of the bath, the probability of the atomic excited state will appear to be periodic oscillations with a single frequency, i.e., regular oscillations, indicating that the hybrid system made up of the

*These authors contributed equally to this work.

†aiqing@bnu.edu.cn

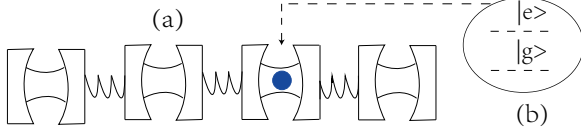


FIG. 1. Schematic illustration of a two-level atom and a coupled-cavity array. (a) Structure of coupled cavities and (b) a two-level atom.

atom and the coupled resonators is in a bound state at this time. Therefore, the bound state is the superposition of the atomic excited state and photons localized in a few cavities around the cavity where the atom exists. The duration of the regular oscillations is finite and is determined by the number of cavities in the coupled-cavity array. In this case, we find that the uncertainty of the measured transition frequency of the atom decreases over coding time as t^{-1} on the duration of the regular oscillations.

This paper is organized as follows. In the next section, we introduce our simulation scheme. By using N qubits, we can effectively simulate the quantum dynamics of one atom and $2^N - 1$ coupled cavities. We also provide the probability of the atomic excited state and the standard deviation of the measured atomic transition frequency, detailed derivations of which are shown in Appendixes A and B, respectively. Then, in Sec. III, we use the direct mapping method, which is given in Appendix C, to numerically simulate the dynamics of the atomic excited state. We explore the relation between the duration, frequency, amplitude, and mean of the regular oscillations and the number of cavities. We use both analytical and numerical methods to verify that the error of the measurement decreases over time in the presence of a bound state. We find that the standard deviation of the measured atomic transition frequency on the scale t^{-1} can be achieved. In Sec. IV, we summarize our main findings.

II. SCHEME

We consider the interaction between a two-level atom and a coupled-cavity array [56]. As shown in Fig. 1, the Hamiltonian of the system reads

$$H = H_0 + H_I, \quad (1)$$

$$H_0 = \Omega|e\rangle\langle e| + \sum_{j=-j_M}^{j_M} [\omega_0 a_j^\dagger a_j - \xi(a_j^\dagger a_{j+1} + a_{j+1}^\dagger a_j)], \quad (2)$$

$$H_I = J(a_0^\dagger \sigma_- + a_0 \sigma_+), \quad (3)$$

where Ω is the transition frequency of the atom; a_j^\dagger (a_j) creates (annihilates) a photon with frequency ω_0 in the j th cavity; ξ is the coupling constant between two adjacent resonators; $\sigma_+ = |e\rangle\langle g| = (\sigma_-)^\dagger$ is the raising operator of the atom, with $|e\rangle$ and $|g\rangle$ being the excited and ground states of the atom, respectively; J is the coupling constant between the atom and the zeroth cavity; n is the total number of cavities; and $j_M = (n - 1)/2$. In this paper, we assume $\hbar = 1$ for simplicity.

Assuming a periodical boundary condition, by Fourier transformation, i.e., $a_j^\dagger = \sum_k a_k^\dagger e^{ikj}/\sqrt{n}$, the total

Hamiltonian (1) can be rewritten as

$$H = \sum_k \omega_k a_k^\dagger a_k + \Omega|e\rangle\langle e| + \sum_k J_k(a_k^\dagger \sigma_- + \text{H.c.}), \quad (4)$$

where $\omega_k = \omega_0 - 2\xi \cos(k)$ and $J_k = J/\sqrt{n}$. Since the total excitation $\mathcal{N} = \sum_k a_k^\dagger a_k + |e\rangle\langle e|$ is conserved, i.e., $[H, \mathcal{N}] = 0$, we assume that at time t the system is in the state $|\psi(t)\rangle = \alpha(t)|v, e\rangle + \sum_k \beta_k(t)a_k^\dagger|v, g\rangle$, with $|v\rangle$ being the vacuum state of all the cavities. According to the Schrödinger equation, we have

$$i\dot{\alpha} = \Omega\alpha + \sum_k J_k \beta_k, \quad (5)$$

$$i\dot{\beta}_k = \omega_k \beta_k + J_k \alpha, \quad (6)$$

where the initial condition is given as $\alpha(0) = 1$, $\beta_k(0) = 0$. As shown in Appendix A, we can obtain the analytic expression of the probability amplitude of the excited state of the atom as

$$\alpha(t) = A_1 e^{p_1 t} + A_2 e^{p_2 t} + \int_{-2\xi}^{2\xi} C(x) e^{i(x-\omega_0)t} dx, \quad (7)$$

where A_j ($j = 1, 2$) are real and p_j ($j = 1, 2$) are imaginary. The explicit expressions for all these parameters, including $C(x)$, can be found in Appendix A. Since the last term in Eq. (7) decays exponentially in the long-time limit, the probability of the excited state of the atom reads

$$P_e = |\alpha(\infty)|^2 = A_1^2 + A_2^2 + 2A_1 A_2 \cos(\phi t), \quad (8)$$

where $\phi = ip_2 - ip_1$. In order to measure the atomic transition frequency precisely, the variance is determined by the quantum Fisher information $F(\Omega)$ as [28,57,58]

$$\delta\Omega^2 = \frac{1}{(T/t)F(\Omega)}, \quad (9)$$

$$F(\Omega) \equiv \frac{1}{P_e(1-P_e)} \left(\frac{\partial P_e}{\partial \Omega} \right)^2, \quad (10)$$

where T is the total duration of the experiment which is separated into different repetitions of duration t . Using the perturbation theory, as shown in Appendix B, we have

$$\phi = 4\xi + \frac{(\omega_0 - \Omega)^2 + 4\xi^2}{2\xi[(\omega_0 - \Omega)^2 - 4\xi^2]} J^4. \quad (11)$$

By inserting Eqs. (8), (10), and (11) into Eq. (9), we can obtain the uncertainty of the atomic transition frequency as

$$\delta\Omega^2 = \frac{t\xi^2 B_1 B_2}{J^8 T B_3}, \quad (12)$$

where

$$B_1 = -\frac{J^8}{4\Omega_-^6 \xi^2} - \frac{J^8}{4\Omega_+^6 \xi^2} + \frac{J^8 \cos(\phi t)}{2\Omega_-^3 \Omega_+^3 \xi^2} + 1, \quad (13)$$

$$B_2 = \frac{1}{\Omega_-^6} + \frac{1}{(\Omega_+)^6} - \frac{2 \cos(\phi t)}{\Omega_-^3 \Omega_+^3}, \quad (14)$$

$$B_3^{1/2} = \frac{J^4 t (\Omega - \omega_0) (12\xi^2 + (\Omega - \omega_0)^2) \sin(\phi t)}{\xi \Omega_-^6 \Omega_+^6} - \frac{3}{\Omega_-^7} - \frac{3}{\Omega_+^7} + \frac{3 \cos(\phi t)}{\Omega_-^4 \Omega_+^3} + \frac{3 \cos(\phi t)}{\Omega_-^3 \Omega_+^4}, \quad (15)$$

with $\Omega_\pm = \pm 2\xi + \omega_0 - \Omega$.

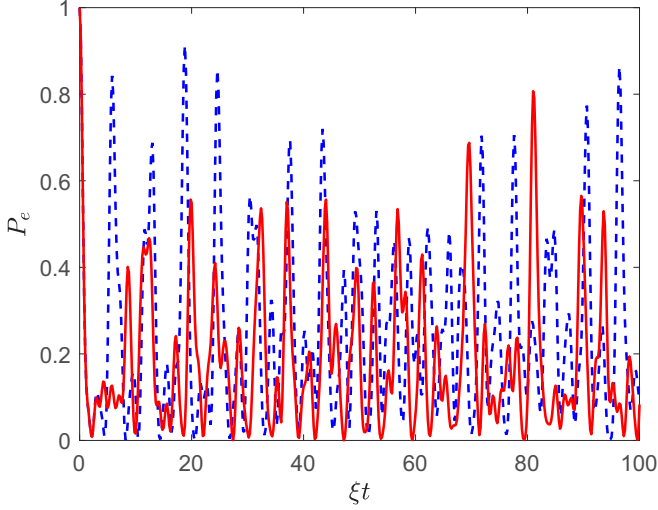


FIG. 2. The population dynamics $P_e(t)$ of an atomic excited state with small N , e.g., $N = 3$ (blue dashed line) and $N = 4$ (red solid line). Here, the parameters used in the calculation are $\omega_0 = 10\xi$, $\Omega = 11\xi$, and $J = 1.3\xi$.

III. NUMERICAL SIMULATION AND DISCUSSION

As shown in Appendix C, we utilize N qubits to effectively simulate the quantum dynamics for one atom interacting with $2^N - 1$ coupled resonators in the single-excitation subspace. Figure 2 shows that when the number of qubits N is relatively small, e.g., $N = 3, 4$, the population of the atom in the excited state $P_e(t)$ does not oscillate with a specific frequency and thus does not provide any information about the frequency of the atom. However, if N is increased, e.g., $N = 6, 7$ in Fig. 3, we find that there are persistent oscillations in $P_e(t)$, which indicates that a bound state in the atom interacting with the

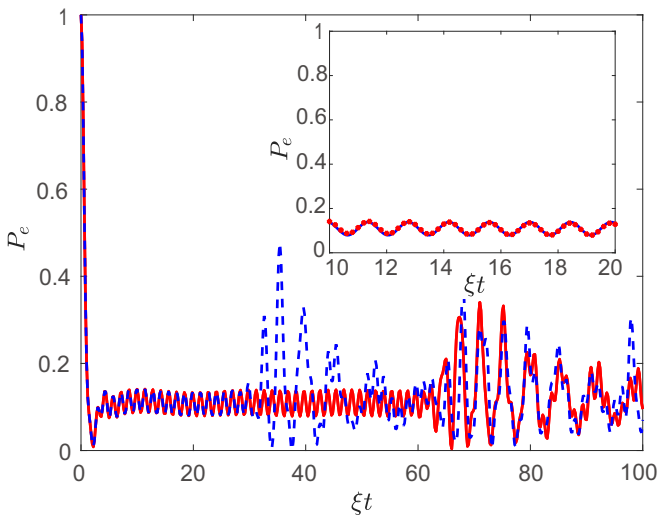


FIG. 3. The population dynamics $P_e(t)$ of an atomic excited state with larger N , e.g., $N = 6$ (blue dashed line) and $N = 7$ (red solid line). The inset compares the numerical simulation of the regular oscillations of the population dynamics $P_e(t)$ with $N = 8$ (red stars) vs the analytical solution (blue solid line) for Eq. (8) over a period of time. Here, the parameters are the same as in Fig. 2.

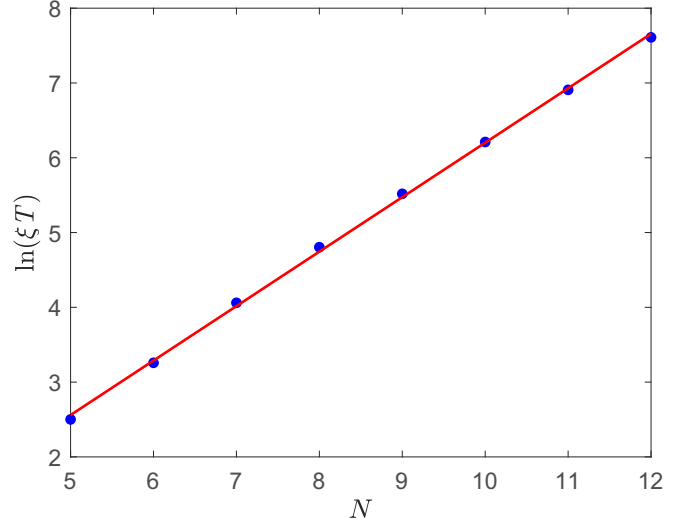


FIG. 4. The duration of the regular oscillations as a function of the number of qubits N . We use the function $\ln(\xi T) = 0.72823N - 1.0812$ (red solid line) to fit the data (blue dots) with the linear correlation coefficient $r = 0.99967$. The other parameters are the same as in Fig. 2.

cavity array exists. The underlying physical mechanism can be explained well by the analytical solution obtained in the previous section; note that the analytical solution we obtained in the previous section was obtained under the assumption of infinite N . At the beginning, due to the third term in Eq. (7), $P_e(t)$ oscillates out of order. As time passes, since the contribution from the branch cut vanishes, $P_e(t)$ oscillates with a specific frequency, as predicted by Eq. (8). In the inset of Fig. 3, the numerical simulation and fitting results for Eq. (8) are compared. The results in Fig. 3 show that when N is large enough, e.g., $N = 5$, the population of the excited state of the atom will show a regular oscillation for a period of time. The frequency, the amplitude, and the mean of these regular oscillations are, respectively, ϕ , $2A_1A_2$, and $A_1^2 + A_2^2$ in Eq. (8). According to Eq. (11), ϕ is proportional to J^4 . In contrast to ϕ vs J , the relation between ϕ and ξ is trickier. For a given J , a minimum ϕ as ξ varies exists. As J decreases, the minimum also decreases, and the position of the minimum along the ξ axis approaches closer and closer to the J axis. $A_1^2 + A_2^2$ is insensitive to the variation of ξ and J except when the atom is strongly coupled to the cavity and the cavities are weakly coupled to each other. In this regime, $A_1^2 + A_2^2$ increases sharply as J grows or ξ decreases. The same behavior can also be observed in the relation between $2A_1A_2$ and $J + \xi$. By measuring this frequency of regular oscillations, we effectively obtain the atomic transition frequency. Notice that these regular oscillations do not last forever. Interestingly, the duration of these regular oscillations seems to get longer as N increases.

In order to study the relation between the duration of regular oscillations T and the number of qubits N , we plot $\ln(\xi T)$ vs N in Fig. 4. By a linear fit with the linear correlation coefficient $r = 0.99$, we show that $\xi T = \exp(0.72823N - 1.0812)$, which implies that the duration of the regular oscillations doubles if we use one more qubit, i.e., $\exp(0.72823) \simeq 2.0714$.

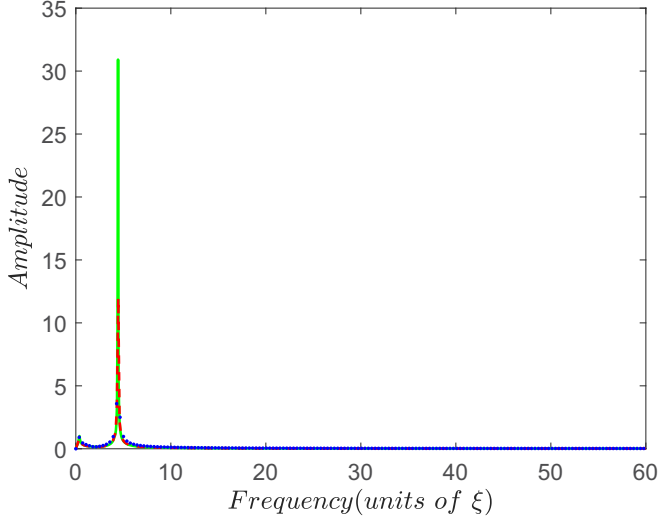


FIG. 5. Fourier transform for the regular oscillations with different qubit numbers. The FWHMs of the main peak are, respectively, 0.288ξ , 0.135ξ , and 0.082ξ for $N = 6$ (blue dotted line), $N = 7$ (red dashed line), and $N = 8$ (green solid line). The other parameters are the same as in Fig. 2.

Thus, we can tune the coding time by varying the number of cavities in the array. This allows us to improve the measurement accuracy to obtain the atomic transition frequency with a much smaller error. When N approaches infinity, the coding time can be infinite, and we can obtain a perfect measurement of the atomic transition frequency [see Eq. (9)]. To study their other properties, we perform the Fourier transform on the regular oscillations, as shown in Fig. 5. There is a clear main peak at 4.42ξ . We can see that as the number of qubits N increases, the height of the main peak is significantly enlarged, and its full width at half maximum (FWHM) is reduced. This implies that the regular oscillations become more regular when N approaches infinity. We also notice that in addition to the main peak, there is a much smaller peak at 0.35ξ . This suggests that the bound state is made up of an atomic excitation and photons in a few cavities. In Fig. 6, we show both the amplitude and mean of the regular oscillations. As the number of qubits N increases, both the amplitude and mean of the regular oscillations approach the ones with infinite N obtained with the analytical solution given in Eq. (8). The results shown in Figs. 5 and 6 suggest that the greater the number of qubits the system is composed of, the more stable the bound state appears, and thus, the smaller the error that we obtain when we measure the transition frequency of the atom is. As shown in Figs. 7 and 8 below, we apply both the analytical and numerical methods to confirm our conjecture that bound states can help us improve the accuracy of the measurements.

In Fig. 7, by the red solid line, we show the uncertainty of the atomic transition frequency $\delta\Omega$ obtained with Eq. (12) when the atomic transition frequency is within the band of the coupled resonators. At first, $\delta\Omega$ experiences a rapid rise, followed by a slow decay, guaranteeing the recovery of the vanishing measurement error. Note that in obtaining Eq. (12) we assume that the atom-resonator coupling J is weak, i.e.,

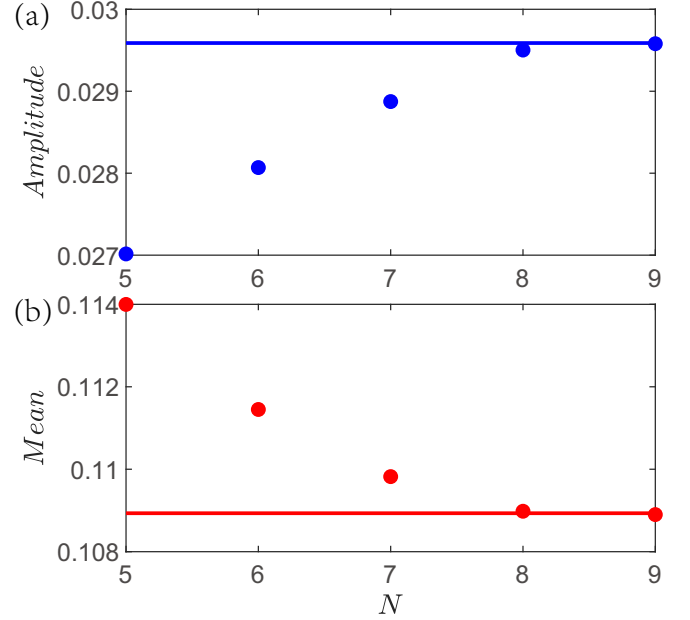


FIG. 6. (a) The amplitude of the regular oscillations for different numbers of qubits N obtained with the numerical simulation (blue dots) is compared to the one with infinite N obtained with the analytical solution (blue solid line). (b) The mean of the regular oscillations for different numbers of qubits N obtained with the numerical simulation (red dots) is compared to the one with infinite N obtained with the analytical solution (red solid line). The other parameters are the same as in Fig. 2.

$|\omega_0 \pm 2\xi|$, $\Omega \gg J$, and the atomic transition frequency is within the band of the coupled resonators, i.e., $\Omega \in [\omega_0 - 2\xi, \omega_0 + 2\xi]$. In order to verify that the above assumption is valid, we compare the approximated Eq. (12) with numeri-

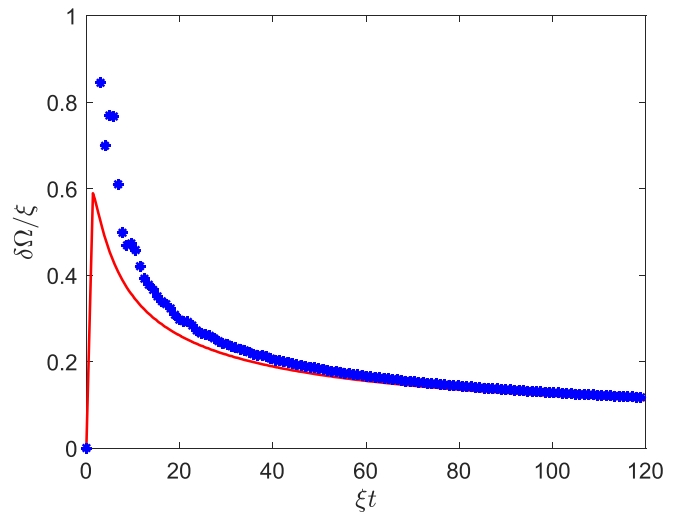


FIG. 7. Comparison of analytical and numerical results for the uncertainty $\delta\Omega$ vs time. The red solid line is obtained with Eq. (12), while the blue stars are obtained with the numerically exact solution with the following parameters: $N = 8$, $\omega_0 = 20\xi$, $\Omega = 20.5\xi$, and $J = 3\xi$. With the selection of N , the regular oscillations for the probability of the atomic excited state stop at $\xi T = 120$.

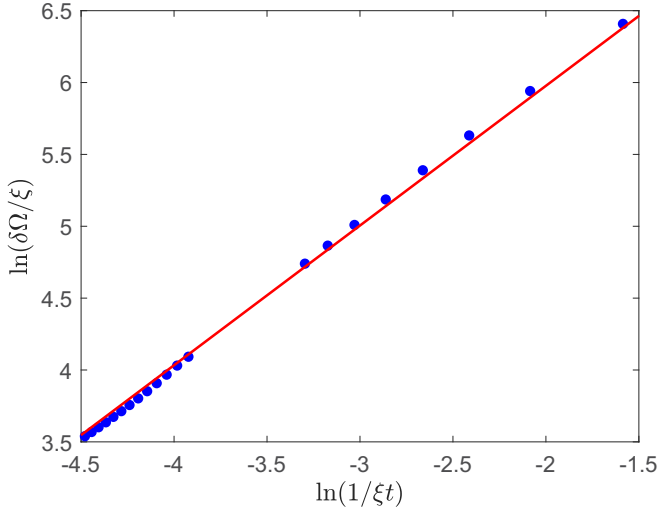


FIG. 8. The scaling of the uncertainty $\delta\Omega$ vs time. The blue dots are obtained with the numerical solution with the following parameters: $N = 8$, $\omega_0 = 20\xi$, $\Omega = 20\xi$, and $J = 0.3\xi$. The red solid line is obtained by fitting the data with the function $\ln(\delta\Omega/\xi) = 0.97196 \times \ln(1/\xi t) + 7.9211$ and the linear correlation coefficient $r = 0.9995$.

cally exact Eq. (9) in Fig. 7. Obviously, the two solutions agree very well with each other, which suggests reliable approximations were made in Eq. (12). In noiseless metrology, the standard deviation of the measured transition frequency scales as t^{-1} with respect to the time. In Fig. 8, we investigate the standard deviation at the optimal measurement times. By linear fitting, we numerically demonstrate that $\delta\Omega \propto t^{-1}$ up to $\xi T = 120$, which is the duration of the regular oscillations. However, due to the limitation of the approximations of the analytical method, we cannot effectively simulate the situation with an atomic transition frequency beyond the band using Eq. (12). In Fig. 9, we plot the dynamics of the measured atomic transition frequency using Eq. (9) with the parameters

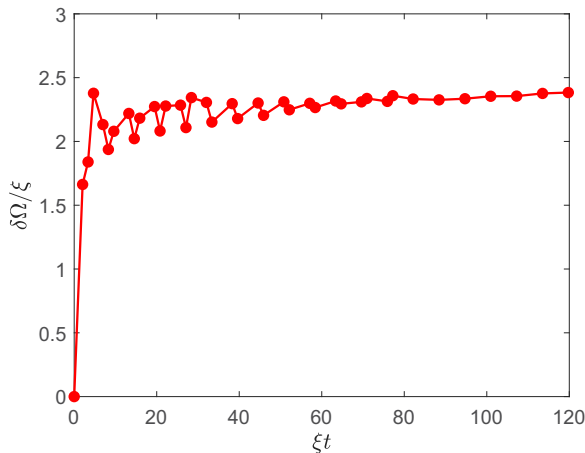


FIG. 9. Numerical simulation of the uncertainty $\delta\Omega$ vs time with the measured atomic transition frequency Ω beyond the band of the coupled resonators. The data are obtained with Eq. (9) with the following parameters: $N = 8$, $\Omega = 17\xi$, $\omega_0 = 10\xi$, $J = 0.3\xi$, and $\xi T = 120$.

$N = 8$, $\Omega = 17\xi$, $\omega_0 = 10\xi$, $J = 0.3\xi$, and $\xi T = 120$. As shown, after an increase of about $\xi t = 50$, $\delta\Omega$ achieves a steady state, although oscillations with small amplitude still exist. It does not recover the $1/t$ measurement because the bound state does not exist.

IV. CONCLUSION

To conclude, we studied the effects of the bound state on quantum metrology in an atom interacting with coupled resonators. In a hybrid system with a finite number n of cavities, we found that when the number of qubits is large enough, e.g., $n \geq 2^5 - 1 = 31$, regular oscillations in the population dynamics of the atomic excited state, which may be used to evaluate the atomic transition frequency, exist. The duration of these regular oscillations is linear with respect to n . For a given n , we showed that during the duration of the regular oscillations, the standard deviation of the measured atomic transition frequency is inversely proportional to t . If more cavities are involved, since the duration of the regular oscillations gets longer, the measured atomic transition frequency will become more and more accurate. These regular oscillations indicate that a bound state exists in the hybrid system. Their duration lasts for a finite time because there are finite cavities, i.e., finite bath modes. Using numerical simulations, we proved that the bound state exists when the atomic transition frequency is within the energy band of the coupled resonators. In addition to the numerical simulations, we obtained an analytical result for the uncertainty of the atomic transition frequency for small atom-cavity interaction strength when the bound state is present. It indicates that the error-free measurement is recovered with infinite cavities in the long-time limit due to the existence of the bound state. The results suggest that the non-Markovian effects and the bound state account for the high accuracy of quantum metrology. Our research may shed light on the design of the hybrid system for exploring the bound state for quantum metrology.

ACKNOWLEDGMENTS

This work is supported by the Innovation Program for Quantum Science and Technology under Grant No. 2023ZD0300200, the Beijing Natural Science Foundation under Grant No. 1202017, the National Natural Science Foundation of China under Grants No. 11674033 and No. 11505007, Beijing Normal University under Grant No. 2022129, the Scientific and Technological Research Program of the Chongqing Municipal Education Commission under Grant No. KJQN202200603, and Chongqing University of Posts and Telecommunications under Grant No. A2022-304.

APPENDIX A: POPULATION OF THE ATOMIC EXCITED STATE

After the Fourier transformation, the total Hamiltonian reads [59]

$$H = \sum_k \omega_k a_k^\dagger a_k + \Omega |e\rangle \langle e| + \sum_k J_k a_k^\dagger \sigma_- + \text{H.c.} \quad (\text{A1})$$

In the subspace of a single excitation, we assume the wave function is

$$|\psi\rangle = \alpha(t)|0, e\rangle + \sum_k \beta_k(t)|k, g\rangle. \quad (\text{A2})$$

By inserting Eqs. (A2) and (A1) into the Schrödinger equation, we can obtain

$$i\dot{\alpha}(t) = \Omega\alpha(t) + \sum_k J_k \beta_k(t), \quad (\text{A3})$$

$$i\dot{\beta}_k(t) = \omega_k \beta_k(t) + J_k \alpha(t), \quad (\text{A4})$$

where $\alpha(0) = 1$ and $\beta_k(0) = 0$ are the initial conditions of the system. Then, we perform the Laplace transform on Eqs. (A3) and (A4) and get

$$i[p\tilde{\alpha}(p) - 1] = \Omega\tilde{\alpha}(p) + \sum_k J_k \tilde{\beta}_k(p), \quad (\text{A5})$$

$$ip\tilde{\beta}_k(p) = \omega_k \tilde{\beta}_k(p) + J_k \tilde{\alpha}(p). \quad (\text{A6})$$

After some algebra, we can calculate the probability amplitude of the excited state in p space as

$$\tilde{\alpha}(p) = \frac{1}{p+i\Omega + \sum_k \frac{J_k^2}{p+i\omega_k}}. \quad (\text{A7})$$

After the inverse Laplace transformation, we can obtain the probability amplitude of the excited state in the time domain as

$$\alpha(t) = \frac{1}{2\pi i} \int_{\sigma-i\infty}^{\sigma+i\infty} dp \tilde{\alpha}(p) e^{pt}. \quad (\text{A8})$$

Using the residual theorem, we have

$$\begin{aligned} \alpha(t) = & -\frac{1}{2\pi i} \left(\int_{C_R} \tilde{\alpha}(p) e^{pt} + \int_{l_1} \tilde{\alpha}(p) e^{pt} + \int_{l_2} \tilde{\alpha}(p) e^{pt} \right) \\ & + \sum_{j=1}^2 \text{res}[\tilde{\alpha}(p_j) e^{p_j t}], \end{aligned} \quad (\text{A9})$$

where C_R is a large semicircle at infinity and p_j and l_j ($j = 1, 2$) are, respectively, the two singularities and two branch lines, which are given by

$$p + i\Omega + \sum_k \frac{J_k^2}{p + i\omega_k} = 0. \quad (\text{A10})$$

According to Eq. (A10), the branch lines are defined by $p + i\omega_k = 0$, i.e., $p \in [ip_m, ip_M]$, where $p_m = -\omega_0 - 2\xi$ and $p_M = -\omega_0 + 2\xi$. Note that

$$\sum_k \frac{J_k^2}{p + i\omega_k} = \frac{J^2}{2\pi\xi} \oint_{|z|=1} dz \frac{1}{z^2 + \mathcal{M}z + 1}, \quad (\text{A11})$$

where $\mathcal{M} = (ip - \omega_0)/\xi$ and $z_{\pm} = (-\mathcal{M} \pm \sqrt{\mathcal{M}^2 - 4})/2$ are the two singularities. In other words, $p \notin [-i(\omega_0 + 2\xi), -i(\omega_0 - 2\xi)]$, i.e., $\mathcal{M} > 2$ or $\mathcal{M} < -2$. In the former case, since $ip > \omega_0 + 2\xi$ and $-1 < z_+ < 0$, $z_- < -1$, we have

$$\frac{J^2}{2\pi\xi} \oint_{|z|=1} dz \frac{1}{z^2 + \mathcal{M}z + 1} = \frac{iJ^2}{\xi\sqrt{\mathcal{M}^2 - 4}}. \quad (\text{A12})$$

By substituting Eq. (A12) into Eq. (A10), we can obtain

$$p + i\Omega + i \frac{J^2}{\xi\sqrt{\mathcal{M}^2 - 4}} = f_1(p). \quad (\text{A13})$$

With $f_1(p_1) = 0$ and $ip_1 > \omega_0 + 2\xi$, we attain the first singularity. In the same way, for the case of $\mathcal{M} < -2$, since

$$\frac{J^2}{2\pi\xi} \oint_{|z|=1} \frac{dz}{z^2 + \mathcal{M}z + 1} = -\frac{iJ^2}{\xi\sqrt{\mathcal{M}^2 - 4}}, \quad (\text{A14})$$

we have

$$p + i\Omega - i \frac{J^2}{\xi\sqrt{\mathcal{M}^2 - 4}} = f_2(p). \quad (\text{A15})$$

With $f_2(p_2) = 0$ and $ip_2 < \omega_0 - 2\xi$, we can obtain the second singularity. As a result, the contribution from the singularities in Eq. (A9) reads

$$\text{res}(\tilde{\alpha}(p_j) e^{p_j t}) = A_j e^{p_j t}, \quad (\text{A16})$$

where $A_j = \left(\frac{df_j}{dp}\bigg|_{p_j}\right)^{-1}$.

Thanks to Jordan's lemma, we know $\int_{C_R} \tilde{\alpha}(p) e^{pt} = 0$. Thus, we have

$$\begin{aligned} & -\frac{1}{2\pi i} \left(\int_{l_1} \tilde{\alpha}(p) e^{pt} + \int_{l_2} \tilde{\alpha}(p) e^{pt} dp \right) \\ & = -\frac{1}{2\pi i} \left(\int_{p_m}^{p_M} \frac{e^{ipt}}{p + \Omega - \sum_k \frac{J_k^2}{p + i\omega_k + i0^+}} dp \right. \\ & \quad \left. + \int_{p_M}^{p_m} \frac{e^{ipt}}{p + \Omega - \sum_k \frac{J_k^2}{p + i\omega_k - i0^+}} dp \right). \end{aligned} \quad (\text{A17})$$

Here,

$$\begin{aligned} \sum_k \frac{J_k^2}{p + i\omega_k \pm i0^+} = & \frac{J^2}{2\pi} \left[\mp \frac{i2\pi}{\sqrt{4\xi^2 - (\omega_0 + p)^2}} \right. \\ & \left. + \int_{-\pi}^{\pi} dk P\left(\frac{1}{p + \omega_k}\right) \right], \end{aligned} \quad (\text{A18})$$

where $P(x)$ is the principal-value function. Since

$$\int_{-\pi}^{\pi} dk P\left(\frac{1}{p + \omega_k}\right) = 0, \quad (\text{A19})$$

by inserting Eq. (A18) into Eq. (A17), we have

$$-\frac{1}{2\pi i} \left(\int_{l_1} \tilde{\alpha}(p) e^{pt} + \int_{l_2} \tilde{\alpha}(p) e^{pt} dp \right) = \int_{-2\xi}^{2\xi} C(x) e^{i(x-\omega_0)t} dx, \quad (\text{A20})$$

where $C(x) = (g^2 \sqrt{4\xi^2 - x^2}) / \{(\Omega - \omega_0 + x)^2 [4\xi^2 - (x)^2] + g^4\}$. Finally, we obtain the probability amplitude of the atomic excited state as

$$\alpha(t) = A_1 e^{p_1 t} + A_2 e^{p_2 t} + \int_{-2\xi}^{2\xi} C(x) e^{i(x-\omega_0)t} dx, \quad (\text{A21})$$

where

$$A_j = \frac{(ip_j - \omega_0)^2 - 4\xi^2}{(ip_j - \omega_0)^2 - 4\xi^2 + (ip_j - \Omega)(ip_j - \omega_0)}. \quad (\text{A22})$$

After some algebra, we find that p_j ($j = 1, 2$) are pure imaginary numbers.

APPENDIX B: UNCERTAINTY BY PERTURBATION

In order to obtain the uncertainty of Ω , we first determine p_1 and p_2 in Eq. (A21) using perturbation theory. Take advantage of Eqs. (A13) and (A15), we have

$$(ip - \Omega)^2[(ip - \omega_0)^2 - 4\xi^2] = J^4. \quad (\text{B1})$$

By the perturbation theory, to the zeroth order of J^4 , we can obtain

$$(x - \Omega)^2[(x - \omega_0)^2 - 4\xi^2] = 0, \quad (\text{B2})$$

where $x = ip$. There are three solutions to the above equation, i.e.,

$$x_{01} = \omega_0 + 2\xi, \quad (\text{B3})$$

$$x_{02} = \omega_0 - 2\xi, \quad (\text{B4})$$

$$x_{03} = x_{04} = \Omega. \quad (\text{B5})$$

In the following, we obtain the solutions to Eq. (B1) to the first order of J^4 .

As shown in Appendix A, $ip_1 > 2\xi + \omega_0$, and $ip_2 < -2\xi + \omega_0$; only x_1 and x_2 are retained for the following discussion. To the first order of J^4 , we assume $x_j = x_{0j} + C_j J^4$ ($j = 1, 2, 3, 4$). Inserting them back into Eq. (B1), we can obtain

$$(x - \Omega)^2(x - x_{01})(x - x_{02}) = J^4. \quad (\text{B6})$$

Thus, we have

$$C_1 = \frac{1}{4\xi\Omega_+^2}, \quad (\text{B7})$$

$$C_2 = \frac{-1}{4\xi\Omega_-^2}, \quad (\text{B8})$$

where $\Omega_{\pm} = \pm 2\xi + \omega_0 - \Omega$. In all, $p_1 = -ix_1$, and $p_2 = -ix_2$.

Now that we know the analytical expressions of p_j , in the long-time limit, the population of the atom in the excited state reads

$$P_e = |\alpha(\infty)|^2 = A_1^2 + A_2^2 + 2A_1A_2 \cos(\phi t), \quad (\text{B9})$$

where $\phi = x_1 - x_2$; the contribution from the integral term in Eq. (A21) vanishes when the time is large enough. By inserting p_1 and p_2 into Eq. (A22), we have

$$A_1 = \frac{J^4}{2\Omega_+^3\xi}, \quad (\text{B10})$$

$$A_2 = -\frac{J^4}{2\Omega_-^3\xi}, \quad (\text{B11})$$

$$\phi = 4\xi + (C_1 - C_2)J^4. \quad (\text{B12})$$

The uncertainty of the atomic transition frequency is written as

$$\delta\Omega^2 = \frac{1}{(T/t)F(\Omega)}, \quad (\text{B13})$$

where the Fisher information $F(\Omega)$ is

$$F(\Omega) \equiv \frac{1}{P_e(1 - P_e)} \left(\frac{\partial P_e}{\partial \Omega} \right)^2. \quad (\text{B14})$$

According to Eqs. (B13), (B14), and (B9), the uncertainty is explicitly given as

$$\delta\Omega^2 = \frac{t\xi^2 B_1 B_2}{J^8 T B_3}, \quad (\text{B15})$$

where

$$B_1 = -\frac{J^8}{4\Omega_-^6\xi^2} - \frac{J^8}{4\Omega_+^6\xi^2} + \frac{J^8 \cos(\phi t)}{2\Omega_-^3\Omega_+^3\xi^2} + 1, \quad (\text{B16})$$

$$B_2 = \frac{1}{\Omega_-^6} + \frac{1}{(\Omega_+)^6} - \frac{2 \cos(\phi t)}{\Omega_-^3\Omega_+^3}, \quad (\text{B17})$$

$$B_3^{1/2} = \frac{J^4 t (\Omega - \omega_0) [12\xi^2 + (\Omega - \omega_0)^2] \sin(\phi t)}{\xi \Omega_-^6 \Omega_+^6} - \frac{3}{\Omega_-^7} - \frac{3}{\Omega_+^7} + \frac{3 \cos(\phi t)}{\Omega_-^4 \Omega_+^3} + \frac{3 \cos(\phi t)}{\Omega_-^3 \Omega_+^4}. \quad (\text{B18})$$

APPENDIX C: DIRECT MAPPING

In this section, we discuss how to demonstrate the bound-state enhanced metrology using the quantum simulation approach with a finite number of qubits. We focus our investigation on the single-excitation subspace. If we use N qubits for quantum simulation, the dimension of the Hilbert space is 2^N . For example, when $N = 2$, we perform the following mapping before carrying out the quantum simulation:

$$|00\rangle = |0\rangle|e\rangle, \quad (\text{C1})$$

$$|01\rangle = a_1^\dagger |0\rangle|g\rangle, \quad (\text{C2})$$

$$|10\rangle = a_2^\dagger |0\rangle|g\rangle, \quad (\text{C3})$$

$$|11\rangle = a_3^\dagger |0\rangle|g\rangle, \quad (\text{C4})$$

where $|g\rangle$ ($|e\rangle$) is the atomic ground (excited) state, $|0\rangle$ is the vacuum state of all cavities, and $a_j^\dagger |0\rangle$ indicates that there is one photon in the j th cavity while all other cavities are in the vacuum state. Therefore, by using N qubits, we can effectively simulate the quantum dynamics of one atom plus $2^N - 1$ coupled cavities.

[1] H. Grote, K. Danzmann, K. L. Dooley, R. Schnabel, J. Slutsky, and H. Vahlbruch, First long-term application of squeezed states

of light in a gravitational-wave observatory, *Phys. Rev. Lett.* **110**, 181101 (2013).

- [2] R. Schnabel, N. Mavalvala, D. E. McClelland, and P. K. Lam, Quantum metrology for gravitational wave astronomy, *Nat. Commun.* **1**, 121 (2010).
- [3] The LIGO Scientific Collaboration, A gravitational wave observatory operating beyond the quantum shot-noise limit, *Nat. Phys.* **7**, 962 (2011).
- [4] S. Barzanjeh, S. Guha, C. Weedbrook, D. Vitali, J. H. Shapiro, and S. Pirandola, Microwave quantum illumination, *Phys. Rev. Lett.* **114**, 080503 (2015).
- [5] L. Maccone and C. L. Ren, Quantum radar, *Phys. Rev. Lett.* **124**, 200503 (2020).
- [6] G. Arrad, Y. Vinkler, D. Aharonov, and A. Retzker, Increasing sensing resolution with error correction, *Phys. Rev. Lett.* **112**, 150801 (2014).
- [7] I. Kruse, K. Lange, J. Peise, B. Lücke, L. Pezzè, J. Arlt, W. Ertmer, C. Lisdat, L. Santos, A. Smerzi, and C. Klempt, Improvement of an atomic clock using squeezed vacuum, *Phys. Rev. Lett.* **117**, 143004 (2016).
- [8] O. Hosten, N. J. Engelsen, R. Krishnakumar, and M. A. Kasevich, Measurement noise 100 times lower than the quantum-projection limit using entangled atoms, *Nature (London)* **529**, 505 (2016).
- [9] L. Pezzè and A. Smerzi, Heisenberg-limited noisy atomic clock using a hybrid coherent and squeezed state protocol, *Phys. Rev. Lett.* **125**, 210503 (2020).
- [10] R. Kaubruegger, D. V. Vasilyev, M. Schulte, K. Hammerer, and P. Zoller, Quantum variational optimization of Ramsey interferometry and atomic clocks, *Phys. Rev. X* **11**, 041045 (2021).
- [11] L. Thiel, D. Rohner, M. Ganzhorn, P. Appel, E. Neu, B. Müller, R. Kleiner, D. Koelle, and P. Maletinsky, Quantitative nanoscale vortex imaging using a cryogenic quantum magnetometer, *Nat. Nanotechnol.* **11**, 677 (2016).
- [12] J. M. Taylor, P. Cappellaro, L. Childress, L. Jiang, D. Budker, P. R. Hemmer, A. Yacoby, R. Walsworth, and M. D. Lukin, High-sensitivity diamond magnetometer with nanoscale resolution, *Nat. Phys.* **4**, 810 (2008).
- [13] H. Bao, J. L. Duan, S. C. Jin, X. D. Lu, P. X. Li, W. Z. Qu, M. F. Wang, I. Novikova, E. E. Mikhailov, K. F. Zhao, K. Mølmer, H. Shen, and Y. H. Xiao, Spin squeezing of 10^{11} atoms by prediction and retrodiction measurements, *Nature (London)* **581**, 159 (2020).
- [14] K. S. Hardman, P. J. Everitt, G. D. McDonald, P. Manju, P. B. Wigley, M. A. Sooriyabandara, C. C. N. Kuhn, J. E. Debs, J. D. Close, and N. P. Robins, Simultaneous precision gravimetry and magnetic gradiometry with a Bose-Einstein condensate: A high precision, quantum sensor, *Phys. Rev. Lett.* **117**, 138501 (2016).
- [15] P. Asenbaum, C. Overstreet, T. Kovachy, D. D. Brown, J. M. Hogan, and M. A. Kasevich, Phase shift in an atom interferometer due to spacetime curvature across its wave function, *Phys. Rev. Lett.* **118**, 183602 (2017).
- [16] J. M. Cai and M. B. Plenio, Chemical compass model for avian magnetoreception as a quantum coherent device, *Phys. Rev. Lett.* **111**, 230503 (2013).
- [17] M. A. Taylor and W. P. Bowen, Quantum metrology and its application in biology, *Phys. Rep.* **615**, 1 (2016).
- [18] A. Crespi, M. Lobino, J. C. F. Matthews, A. Politi, C. R. Neal, R. Ramponi, R. Osellame, and J. L. O'Brien, Measuring protein concentration with entangled photons, *Appl. Phys. Lett.* **100**, 233704 (2012).
- [19] M. A. Taylor, J. Janousek, V. Daria, J. Knittel, B. Hage, H.-A. Bachor, and W. P. Bowen, Subdiffraction-limited quantum imaging within a living cell, *Phys. Rev. X* **4**, 011017 (2014).
- [20] C. Y. Cai, Q. Ai, H. T. Quan, and C. P. Sun, Sensitive chemical compass assisted by quantum criticality, *Phys. Rev. A* **85**, 022315 (2012).
- [21] L. P. Yang, Q. Ai, and C. P. Sun, Generalized Holstein model for spin-dependent electron-transfer reactions, *Phys. Rev. A* **85**, 032707 (2012).
- [22] V. Giovannetti, S. Lloyd, and L. Maccone, Advances in quantum metrology, *Nat. Photon.* **5**, 222 (2011).
- [23] Y. S. Wang, C. Chen, and J. H. An, Quantum metrology in local dissipative environments, *New J. Phys.* **19**, 113019 (2017).
- [24] S. S. Szigeti, S. P. Nolan, J. D. Close, and S. A. Haine, High-precision quantum-enhanced gravimetry with a Bose-Einstein condensate, *Phys. Rev. Lett.* **125**, 100402 (2020).
- [25] C. Y. Luo, J. H. Huang, X. D. Zhang, and C. H. Lee, Heisenberg-limited Sagnac interferometer with multiparticle states, *Phys. Rev. A* **95**, 023608 (2017).
- [26] L. Pezzè and A. Smerzi, Entanglement, nonlinear dynamics, and the Heisenberg limit, *Phys. Rev. Lett.* **102**, 100401 (2009).
- [27] J. Joo, W. J. Munro, and T. P. Spiller, Quantum metrology with entangled coherent states, *Phys. Rev. Lett.* **107**, 083601 (2011).
- [28] W. T. He, H. Y. Guang, Z. Y. Li, R. Q. Deng, N. N. Zhang, J. X. Zhao, F. G. Deng, and Q. Ai, Quantum metrology with one auxiliary particle in a correlated bath and its quantum simulation, *Phys. Rev. A* **104**, 062429 (2021).
- [29] S. S. Zhou, M. Z. Zhang, J. Preskill, and L. Jiang, Achieving the Heisenberg limit in quantum metrology using quantum error correction, *Nat. Commun.* **9**, 78 (2018).
- [30] J. Ma, X. G. Wang, C. P. Sun, and F. Nori, Quantum spin squeezing, *Phys. Rep.* **509**, 89 (2011).
- [31] N. J. Engelsen, R. Krishnakumar, O. Hosten, and M. A. Kasevich, Bell correlations in spin-squeezed states of 500 000 atoms, *Phys. Rev. Lett.* **118**, 140401 (2017).
- [32] M. J. Holland and K. Burnett, Interferometric detection of optical phase shifts at the Heisenberg limit, *Phys. Rev. Lett.* **71**, 1355 (1993).
- [33] S. F. Huelga, C. Macchiavello, T. Pellizzari, A. K. Ekert, M. B. Plenio, and J. I. Cirac, Improvement of frequency standards with quantum entanglement, *Phys. Rev. Lett.* **79**, 3865 (1997).
- [34] A. W. Chin, S. F. Huelga, and M. B. Plenio, Quantum metrology in non-Markovian environments, *Phys. Rev. Lett.* **109**, 233601 (2012).
- [35] Y. Matsuzaki, S. C. Benjamin, and J. Fitzsimons, Magnetic field sensing beyond the standard quantum limit under the effect of decoherence, *Phys. Rev. A* **84**, 012103 (2011).
- [36] X. Y. Long, W. T. He, N. N. Zhang, K. Tang, Z. D. Lin, H. F. Liu, X. F. Nie, G. R. Feng, J. Li, T. Xin, Q. Ai, and D.-W. Lu, Entanglement-enhanced quantum metrology in colored noise by quantum Zeno effect, *Phys. Rev. Lett.* **129**, 070502 (2022).
- [37] S. Y. Bai and J. H. An, Floquet engineering to overcome no-go theorem of noisy quantum metrology, *Phys. Rev. Lett.* **131**, 050801 (2023).
- [38] A. Smirne, J. Kołodyński, S. F. Huelga, and R. Demkowicz-Dobrzański, Ultimate precision limits for noisy frequency estimation, *Phys. Rev. Lett.* **116**, 120801 (2016).
- [39] K. Macieszczak, Zeno limit in frequency estimation with non-Markovian environments, *Phys. Rev. A* **92**, 010102(R) (2015).

- [40] K. Yamamoto, S. Endo, H. Hakoshima, Y. Matsuzaki, and Y. Tokunaga, Error-mitigated quantum metrology via virtual purification, *Phys. Rev. Lett.* **129**, 250503 (2022).
- [41] W. Dür, M. Skotiniotis, F. Fröwis, and B. Kraus, Improved quantum metrology using quantum error correction, *Phys. Rev. Lett.* **112**, 080801 (2014).
- [42] I. Rojko, D. Layden, P. Cappellaro, J. Home, and F. Reiter, Bias in error-corrected quantum sensing, *Phys. Rev. Lett.* **128**, 140503 (2022).
- [43] F. Reiter, A. S. Sørensen, P. Zoller, and C. A. Muschik, Dissipative quantum error correction and application to quantum sensing with trapped ions, *Nat. Commun.* **8**, 1822 (2017).
- [44] M. A. C. Rossi, F. Albarelli, D. Tamascelli, and M. G. Genoni, Noisy quantum metrology enhanced by continuous nondemolition measurement, *Phys. Rev. Lett.* **125**, 200505 (2020).
- [45] K. Bai, Z. Peng, H. G. Luo, and J. H. An, Retrieving ideal precision in noisy quantum optical metrology, *Phys. Rev. Lett.* **123**, 040402 (2019).
- [46] T. Shi, Y. H. Wu, A. González-Tudela, and J. I. Cirac, Bound states in Boson impurity models, *Phys. Rev. X* **6**, 021027 (2016).
- [47] J. Bardeen, L. N. Cooper, and J. R. Schrieffer, Theory of superconductivity, *Phys. Rev.* **108**, 1175 (1957).
- [48] T. Holstein, Studies of polaron motion: Part I. the molecular-crystal model, *Ann. Phys. (NY)* **8**, 325 (1959).
- [49] J. T. Shen and S. H. Fan, Coherent single photon transport in a one-dimensional waveguide coupled with superconducting quantum bits, *Phys. Rev. Lett.* **95**, 213001 (2005).
- [50] D. E. Chang, A. S. Sørensen, E. A. Demler, and M. D. Lukin, A single-photon transistor using nanoscale surface plasmons, *Nat. Phys.* **3**, 807 (2007).
- [51] L. Zhou, Z. R. Gong, Y. X. Liu, C. P. Sun, and F. Nori, Controllable scattering of a single photon inside a one-dimensional resonator waveguide, *Phys. Rev. Lett.* **101**, 100501 (2008).
- [52] L. Zhou, L. P. Yang, Y. Li, and C. P. Sun, Quantum routing of single photons with a cyclic three-level system, *Phys. Rev. Lett.* **111**, 103604 (2013).
- [53] L. Zhou, H. Dong, Y. X. Liu, C. P. Sun, and F. Nori, Quantum supercavity with atomic mirrors, *Phys. Rev. A* **78**, 063827 (2008).
- [54] Y. X. Yao and Q. Ai, Optical non-reciprocity in coupled resonators by detailed balance, *Ann. Phys. (Berlin, Ger.)* **535**, 2300135 (2023).
- [55] Z. H. Wang, L. Zhou, Y. Li, and C. P. Sun, Controllable single-photon frequency converter via a one-dimensional waveguide, *Phys. Rev. A* **89**, 053813 (2014).
- [56] K. Y. Bliokh, Y. P. Bliokh, V. Freilikher, S. Savel'ev, and F. Nori, Colloquium: Unusual resonators: Plasmonics, metamaterials, and random media, *Rev. Mod. Phys.* **80**, 1201 (2008).
- [57] H. P. Breuer and F. Petruccione, *The Theory of Open Quantum Systems* (Oxford University Press, New York, 2002).
- [58] P. Liu, P. Wang, W. Yang, G. R. Jin, and C. P. Sun, Fisher information of a squeezed-state interferometer with a finite photon-number resolution, *Phys. Rev. A* **95**, 023824 (2017).
- [59] Q. Ai and J. Q. Liao, Quantum anti-Zeno effect in artificial quantum systems, *Commun. Theor. Phys.* **54**, 985 (2010).